HHS Public Access

Author manuscript

ACS Macro Lett. Author manuscript; available in PMC 2018 September 19.

Published in final edited form as:

ACS Macro Lett. 2017 September 19; 6(9): 1005–1012. doi:10.1021/acsmacrolett.7b00490.

Core-shell Structure and Aggregation Number of Micelles Composed of Amphiphilic Block Copolymers and Amphiphilic Heterografted Polymer Brushes Determined by Small-Angle X-ray Scattering

Magdalena Szymusiak[§,1], **Joseph Kalkowski**[§,1], **Hanying Luo**[2], **Alexander J. Donovan**[1], **Pin Zhang**[1], **Chang Liu**[1], **Weifeng Shang**[3], **Thomas Irving**[3], **Margarita Herrera-Alonso**[2], and **Ying Liu**[*,1,4]

[1]Department of Chemical Engineering, University of Illinois at Chicago, Chicago, IL 60607, United States

[2]Department of Materials Science and Engineering, Johns Hopkins University, Baltimore, MD 21218, United States

[3]Department of Biological Sciences, Illinois Institute of Technology, Chicago, IL 60616, United States

[4]Department of Biopharmaceutical Sciences, University of Illinois at Chicago, Chicago, IL 60612, United States

Abstract

A large group of functional nanomaterials employed in biomedical applications, including targeted drug delivery, relies on amphiphilic polymers to encapsulate therapeutic payloads via self-assembly processes. Knowledge of the micelle structures will provide critical insights into design of polymeric drug delivery systems. Core-shell micelles composed of linear diblock copolymers poly(ethylene glycol)-*b*-poly(caprolactone) (PEG-*b*-PCL), poly(ethylene oxide)-*b*-poly(lactic acid) (PEG-*b*-PLA), as well as a heterografted brush consisting of a poly(glycidyl methacrylate) backbone with PEG and PLA branches (PGMA-*g*-PEG/PLA) were characterized by dynamic light scattering (DLS) and small angle X-ray scattering (SAXS) measurements to gain structural information regarding the particle morphology, core-shell size, and aggregation number. The structural information at this quasi-equilibrium state can also be used as a reference when studying the kinetics of polymer micellization.

TOC Image

[*]**Corresponding Author**: Address: Department of Chemical Engineering, University of Illinois at Chicago, Rm. 211, 810 S. Clinton St., Chicago IL, 60607, United States, liuying@uic.edu, Tel: (312) 996-8249, Fax: (312) 996-0808.

[§]Equivalent first authors

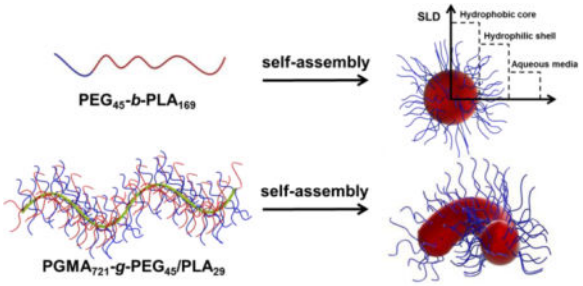

Amphiphilic polymers have become an incredibly important class of polymers due to their spontaneous self-assembly in aqueous solutions into polymeric micelles of core-shell morphology.[1, 2] The core of this particular kind of particle is composed of a collapsed hydrophobic domain of the polymer and the shell consists of the hydrophilic polymer brushes. This core-shell structure of polymeric assemblies has been considered one of the desired structures for targeted drug delivery and sustained release.[3, 4] The particle's hydrophobic core consists of a cargo space for incorporation of the hydrophobic drug into its dense polymer matrix. The outer shell provides steric stability and flexibility for further functionalities. Several linear block copolymers have been incorporated into nanoparticles for drug delivery and medical imaging applications, such as poly(ethylene oxide)-*b*-poly(caprolactone) (PEO-*b*-PCL), poly(ethylene oxide)-*b*-poly(lactic acid) (PEO-*b*-PLA), and poly(lactic acid)-*b*-poly(ethylene oxide)-*b*-poly(lactic acid) (PLA-*b*-PEO-*b*-PLA).[5–7] While simple linear block copolymer micelles have gained considerable attention as robust drug carriers, much less is explored for polymeric core-shell particles composed of more complex macromolecular building blocks such as heterografted brush amphiphiles – a particular class of highly grafted copolymers wherein two different blocks are attached at a block junction in a double-brush architecture. Some initial investigations showed that micelles composed of heterografted brush copolymers had the potential for higher drug encapsulation and sustainable drug release, as compared with their linear analogs.[8] Furthermore, one recent study demonstrated a wide morphological diversity of these structures by manipulating the ratios and lengths of the amphiphilic graft copolymers and their self-assembly conditions.[9]

Physicochemical properties (such as size distribution, surface charge, and gross morphology) of micelles and drug-loaded nanoparticles have been conventionally studied using dynamic light scattering (DLS), static light scattering (SLS), transmission electron microscopy (TEM), zeta-potential measurements, small-angle x-ray scattering (SAXS), and small-angle neutron scattering techniques (SANS).[1, 10, 11] However, for biomedical and biological applications, it is essential to precisely know the structural information at nanometer resolution (i.e. core and shell sizes) in order to optimize drug loading and release schedules and to maintain particle stability. The ability of SAXS to analyze samples in their liquid environments makes it a powerful nanostructure characterization technique. The difference between the electron density of the polymer's hydrophobic and hydrophilic components and the surrounding medium can give sufficient contrast to distinguish unique internal features of the core-shell assemblies. These internal characteristics such as the core size and shell thickness are here of great importance since they directly influence

nanoparticle properties such as drug loading and stability. Larger core size translates into greater cargo space with higher drug loading capability. The shell thickness and the surface density of the hydrophilic polymer impact the nanoparticle dispersion's colloidal stability, as well their biodistribution fate and pharmacokinetic parameters. From the scattering pattern, which is governed by the scattering length density contrast of each part of the polymer and scattering object morphology, size, and polydispersity, detailed information of the micelles can be obtained. There are a few reports employing SAXS to reveal the detailed micellar structures of linear block copolymers, such as Pluronics.[12, 13] Further, no studies to our knowledge report the internal nanostructural features of micelles formed by brush copolymers.

In this study, we have investigated the quasi-equilibrium structures of polymeric micelles that are composed of linear diblock copolymers most commonly used for biomedical applications and, for the first time, more complex macromolecular building block such as heterografted brush polymers. The core-shell-sphere or core-shell-cylinder model was applied to fit the acquired SAXS data and allowed for high structural information content, revealing the size of the core, shell, and the aggregation number of the polymeric micelles. Two ways to regressionally calculate polymer aggregation number were presented. The information provided by this study would direct the rational design of micelles to enhance their function across their possible applications.

Self-assembly of amphiphilic linear diblock copolymers, PEG-*b*-PLA and PEG-*b*-PCL, and heterografted brush copolymer PMGA-*g*-(PEG/PLA) into micelles was achieved by rapid solvent exchange - mixing of polymer tetrahydrofuran (THF) solution with an antisolvent (water) in a multi-inlet-vortex mixer (MIVM). The fast process of flash nanoprecipitation promotes homogenous micro-mixing to produce micelles with narrow size distribution.[14, 15] Structures of the micelles were calculated from the X-ray scattering pattern based on the difference of the scattering length densities of the core, the shell, and the dispersing media (Figure 1D).

The hydrodynamic radius (R_h) of the micelles formed from the linear diblock copolymer was measured using DLS (Table 1). The radius of gyration (R_g) of the polymeric micelles was obtained from SAXS data fitted by the Guinier approximation (Table 1). The particles are considered in the range of Rayleigh scattering. The ratio of R_g and R_h provides insights about the particle compactness and shape – around 0.78 for spherical nanoparticles, and greater than 1 for geometries with disparate length scales, e.g. between radius and length, including over 2 for long wormlike micelles.[16, 17] The calculated ratio of R_g and R_h (R_g/R_h) suggested spherical conformation of the micelles formed from linear diblock copolymers (R_g/R_h~0.78) (Table 1). The structural information derived from these spherical micelles was further examined by fitting the one-dimensional scattering data into core-shell spherical models.

For the amphiphilic copolymer, it is reasonable to consider that a micelle in an aqueous solution is composed of a hydrophobic core (represented by the collapsed hydrophobic part of the polymer) and a hydrophilic shell (represented by the hydrophilic part of the polymer and surrounding water) (Figure 1D). After the solvent-replacement process, the micelles

suspensions were dialyzed for more than 24 hours, and only a trace amount of organic solvent remained in the system, which was not considered during data analysis. The shape of the core-shell architecture is influenced by thermodynamic parameters (such as polymer lengths and ratios of the corresponding blocks of polymers) as well as kinetic control of the self-assembly conditions (such as mixing energy dissipation).[9]

Representing cases of fitting the one-dimensional scattering data of linear diblock copolymers using the core-shell sphere model are shown in Figures 2 and 3. The spherical shape was also confirmed by the near bell shape of the pair-distance distribution function – *p(r)* (Figure 2E, 2F, 3E and 3F). Some deviations from the exact bell-shape were found and are more evident for the PEG_{114}-*b*-PCL_{53} micelles which could be attributed to slightly higher polydispersity of the tested sample. Spherical shape of the particles was also visualized by using TEM (SI, Figure S3). To examine the effects of molecular weights on the structure, PEG length was kept constant while varying the size of PCL for two different molecular weights. For PEG-*b*-PLA, the hydrophobic block of PLA was maintained similar, while changing PEG length.

The calculated structural information of the micelles formed from linear diblock copolymers are listed in Table 2. The difference between the shell SLD from direct model fitting (noted as fitted shell SLD) and the SLD calculated from the PEG percentile resulted from the aggregation number (noted as calculated shell SLD) is listed in the last column in Table 2. More details of model fitting and calculation are presented in the supporting information. The very small discrepancy between the fitted shell SLD and the calculated shell SLD (close to 1% for all cases) validates the calculated aggregation number and the fitting method. With the same size of the PEG hydrophilic block, the core radius increases with an increase of the hydrophobic block polymer length (i.e. PCL) and the aggregation number increases. This observation is consistent with predictions by the scaling and mean-field theories, as well as previous studies on other linear block copolymers.[10, 18, 19] Increasing the length of the PEG block while keeping the PLA block length the same results in the reduction of the nanoparticle core size and aggregation number. Longer PEG chains provide a higher energy barrier and arrest the nanoparticle growth, resulting in a smaller core size.

Amphiphilic heterografted brush copolymers, or amphiphilic graft copolymers, are interesting macromolecular building blocks with a demonstrated ability to self-assemble in aqueous solutions into a variety of polymeric nanostructures.[9, 20] The one particular type of polymer discussed here is composed of a poly(glycidyl methacrylate) (PGMA) backbone with grafted hydrophilic PEG and hydrophobic PLA side-chains (Figure 1C). Effect of concentration and block length of polymers were tested and the conditions are listed in Table 3.

The hydrodynamic radius and the size distribution of the PGMA-*g*-PEG/PLA micelles were measured by DLS (Table 3 and Figure 4). The ratio of R_g and R_h indicated that with the small size of the backbone PGMA the micelles were spherical ($R_g/R_h \sim 0.80$). As the size of the backbone significantly increased, the micelles were elongated to be rod-like (Table 3).

The spherical core-shell model was applied to fit the one-dimensional SAXS data for $PGMA_{68}$-*g*-PEG_{16}/PLA_{17} and $PGMA_{72}$-*g*-PEG_{45}/PLA_{33} micelles (Figure 4B and 4D). The polymers that were used for micelle formation have similar backbone length but differ in arm lengths for both PEG and PLA. The spherical morphology of the micelles was also confirmed by the typical bell shape of the distance-distribution functions, *p(r)* (Figure 4B and 4D) and TEM images (SI, Figure S4). The parameter values obtained from model fitting are reported in Table 4. It was determined that the aggregation numbers of these brush polymers were approximately 4, which is significantly lower compared with the linear diblock copolymer analogs with aggregation numbers one or two orders of magnitude larger. However, the PEG coverage of the micelles formed from the brush copolymer is denser than the linear polymeric micelles. The polymer concentration did not have any influence on the size or other structural parameters of the micelles (Figure S1 and S2, Table 4).

For the micelles composed from the $PGMA_{721}$-*g*-PEG_{45}/PLA_{29} with a long backbone, the core-shell cylinder model was used to fit the scattering data (Figure 4F). The curve of the one-dimensional SAXS data at low Q range indicates that the micelles have elongated rod shapes instead of a sphere, which was confirmed by the ratio of R_h and R_g, the asymmetrical shape of the pair-distribution functions *p(r)* (Figure 4F), and the images by the Cryo-TEM (SI, Figure S5). For an ideal rigid cylinder, the *p(r)* is characterized by the initial bell shape at low *r* followed by the inflection point and a very linear decrease to zero at larger r.[21] The shape of the *p(r)* presented in Figure 4F with the presence of another peak (shoulder) instead of a linear decay toward zero may indicate more flexible rod-like micelles. The parameters obtained from model fitting of the scattering data of $PGMA_{721}$-*g*-PEG_{45}/PLA_{29} micelles are reported in Table 4. It is interesting to note that the calculated aggregation number for this long brush copolymer in aqueous conditions was close to 1 (1.25 for lower particle concentration and 1.55 for higher particle concentration), indicating the presence of unimolecular aggregates. The presence of a long polymer backbone with side PLA chains leads to formation of an elongated micellar morphology. Steric repulsion of the densely grafted PEG side brushes on the long PGMA scaffold promotes intramolecular association.

In summary, we investigated the internal structures of polymeric micelles composed of simple linear diblock copolymers and brush amphiphiles with complex molecular building blocks. The fitting parameters obtained from model fitting the SAXS data revealed the essential internal structural parameters such as the radius and length (in the case of rod-like structures) of the core as well as the shell thickness of the studied micelles. This information was further used to calculate the micelle aggregation numbers, the number of PEG molecules per interfacial area, and the percent PEG content in the shell. Precisely calculating the aggregation number of the micelles is essential for understanding the structure of the micelles and predicting micelles properties, such as drug loading. When measuring micellization kinetics, in the regime of polymer insertion, changes in aggregation number instead of radius of the micelles would yield better sensitivity. The analysis revealed that for the simple linear diblock copolymer intermolecular interactions drive the micelle formation, resulting in relatively large aggregation numbers with lower interfacial density of PEG. On the other hand, for the densely heterografted brush copolymers the intramolecular association of the PLA arm on the PGMA backbone was favored, resulting in near unit aggregation numbers and higher PEG surface density.

Supplementary Material

Refer to Web version on PubMed Central for supplementary material.

Acknowledgments

The research is supported by NSF-CMMI CAREER program to Y.L. (grant # 1350731) and the NSF-DMR CAREER award to M.H.-A. (grant # 11515135).

The research used resources of the Advanced Photon Source, a U.S. Department of Energy (DOE) Office of Science User Facility operated for the DOE Office of Science by Argonne National Laboratory under Contract No. DE-AC02-06CH11357. The majority of the X-ray measurements were performed using facilities of the BioCAT supported by grant 9 P41 GM103622 from the National Institute of General Medical Sciences of the National Institutes of Health. Use of the Pilatus 3 1M detector was provided by grant1S10OD018090-01 from NIGMS.

Measurements on PEG-PLA were performed at the DuPont-Northwestern-Dow Collaborative Access Team (DND-CAT) located at Sector 5 of the Advanced Photon Source (APS). DND-CAT is supported by Northwestern University, E.I. DuPont de Nemours & Co., and The Dow Chemical Company. Data was collected using an instrument funded by the National Science Foundation under Award Number 0960140.

References

1. Riley T, Heald CR, Stolnik S, Garnett MC, Illum L, Davis SS, King SM, Heenan RK, Purkiss SC, Barlow RJ, Gellert PR, Washington C. Core–Shell Structure of PLA–PEG Nanoparticles Used for Drug Delivery. Langmuir. 2003; 19:8428–8435.
2. Gaucher G, Dufresne M-H, Sant VP, Kang N, Maysinger D, Leroux J-C. Block Copolymer Micelles: Preparation, Characterization and Application in Drug Delivery. J Control Release. 2005; 109:169–188. [PubMed: 16289422]
3. Stolnik S, Illum L, Davis SS. Long Circulating Microparticulate Drug Carriers. Adv Drug Deliv Rev. 1995; 16:195–214.
4. Kwon GS, Okano T. Polymeric Micelles as New Drug Carriers. Adv Drug Deliv Rev. 1996; 21:107–116.
5. Hu K, Li J, Shen Y, Lu W, Gao X, Zhang Q, Jiang X. Lactoferrin-Conjugated PEG-PLA Nanoparticles with Improved Brain Delivery: in vitro and in vivo Evaluations. J Control Release. 2009; 134:55–61. [PubMed: 19038299]
6. Peracchia MT, Gref R, Minamitake Y, Domb A, Lotan N, Langer R. PEG-Coated Nanospheres from Amphiphilic Diblock and Multiblock Copolymers: Investigation of their Drug Encapsulation and Release Characteristics. J Control Release. 1997; 46:223–231.
7. Agrawal SK, Sanabria-DeLong N, Coburn JM, Tew GN, Bhatia SR. Novel Drug Release Profiles from Micellar Solutions of PLA–PEO–PLA Triblock Copolymers. J Control Release. 2006; 112:64–71. [PubMed: 16507325]
8. Du J-Z, Tang L-Y, Song W-J, Shi Y, Wang J. Evaluation of Polymeric Micelles from Brush Polymer with Poly(ε-caprolactone)-b-Poly(ethylene glycol) Side Chains as Drug Carrier. Biomacromolecules. 2009; 10:2169–2174. [PubMed: 19722555]
9. Luo HY, Santos JL, Herrera-Alonso M. Toroidal Structures from Brush Amphiphiles. Chem Commun. 2014; 50:536–538.
10. Vangeyte P, Leyh B, Heinrich M, Grandjean J, Bourgaux C, Jerome R. Self-Assembly of Poly(ethylene oxide)-b-poly(ε-caprolactone) Copolymers in Aqueous Solution. Langmuir. 2004; 20:8442–8451. [PubMed: 15379459]
11. Jada A, Hurtrez G, Siffert B, Riess G. Structure of Polystyrene-block-poly(ethylene oxide) Diblock Copolymer Micelles in Water. Macromol Chem Phys. 1996; 197:3697–3710.
12. Manet S, Lecchi A, Imperor-Clerc M, Zholobenko V, Durand D, Oliveira CLP, Pedersen JS, Grillo I, Meneau F, Rochas C. Structure of Micelles of a Nonionic Block Copolymer Determined by SANS and SAXS. J Phys Chem B. 2011; 115:11318–11329. [PubMed: 21863843]

13. Bayati S, Galantini L, Knudsen KD, Schillen K. Complexes of PEO-PPO-PEO Triblock Copolymer P123 and Bile Salt Sodium Glycodeoxycholate in Aqueous Solution: A Small Angle X-ray and Neutron Scattering Investigation. Colloids Surf, A. 2016; 504:426–436.
14. Liu Y, Cheng C, Prud'homme RK, Fox RO. Mixing in a Multi-inlet Vortex Mixer (MIVM) for Flash Nano-precipitation. Chem Eng Sci. 2008; 63:2829–2842.
15. Russ B, Liu Y, Prud'homme RK. Optimized Descriptive Model for Micromixing in a Vortex Mixer. Chem Eng Commun. 2010; 197:1068–1075.
16. Burchard W, Schmidt M, Stockmayer WH. Information on Polydispersity and Branching from Combined Quasi-Elastic and Integrated Scattering. Macromolecules. 1980; 13:1265–1272.
17. Patterson JP, Robin MP, Chassenieux C, Colombani O, O'Reilly RK. The analysis of solution self-assembled polymeric nanomaterials. Chem Soc Rev. 2014; 43:2412–2425. [PubMed: 24519401]
18. Vangeyte P, Leyh B, Auvray L, Grandjean J, Misselyn-Bauduin AM, Jerome R. Mixed Self-Assembly of Poly(ethylene oxide)-b-poly(ε-caprolactone) Copolymers and Sodium Dodecyl Sulfate in Aqueous Solution. Langmuir. 2004; 20:9019–9028. [PubMed: 15461482]
19. Nagarajan R, Ganesh K. Block Copolymer Self-assembly in Selective Solvents: Spherical Micelles with Segregated Cores. J Chem Phys. 1989; 90:5843–5856.
20. Luo H, Szymusiak M, Garcia EA, Lock LL, Cui H, Liu Y, Herrera-Alonso M. Solute-Triggered Morphological Transitions of an Amphiphilic Heterografted Brush Copolymer as a Single-Molecule Drug Carrier. Macromolecules. 2017; 50:2201–2206.
21. Glatter O. The Interpretation of Real-Space Information from Small-Angle Scattering Experiments. J Appl Crystallogr. 1979; 12:166–175.

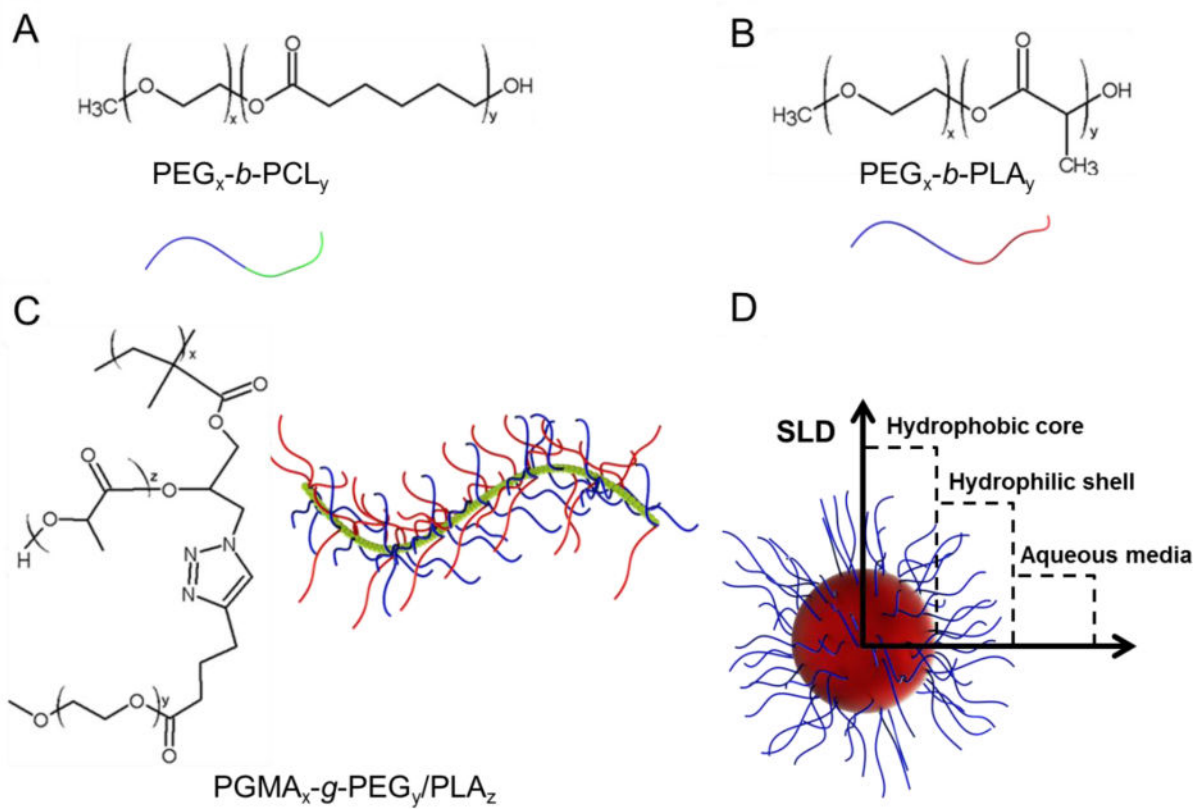

Figure 1.

Molecular structures of the amphiphilic diblock copolymers (A and B) and the heterografted brush copolymers (C) used in the study and their schematic representations. (D) Schematic of scattering length density (SLD) of micellar components in an aqueous environment.

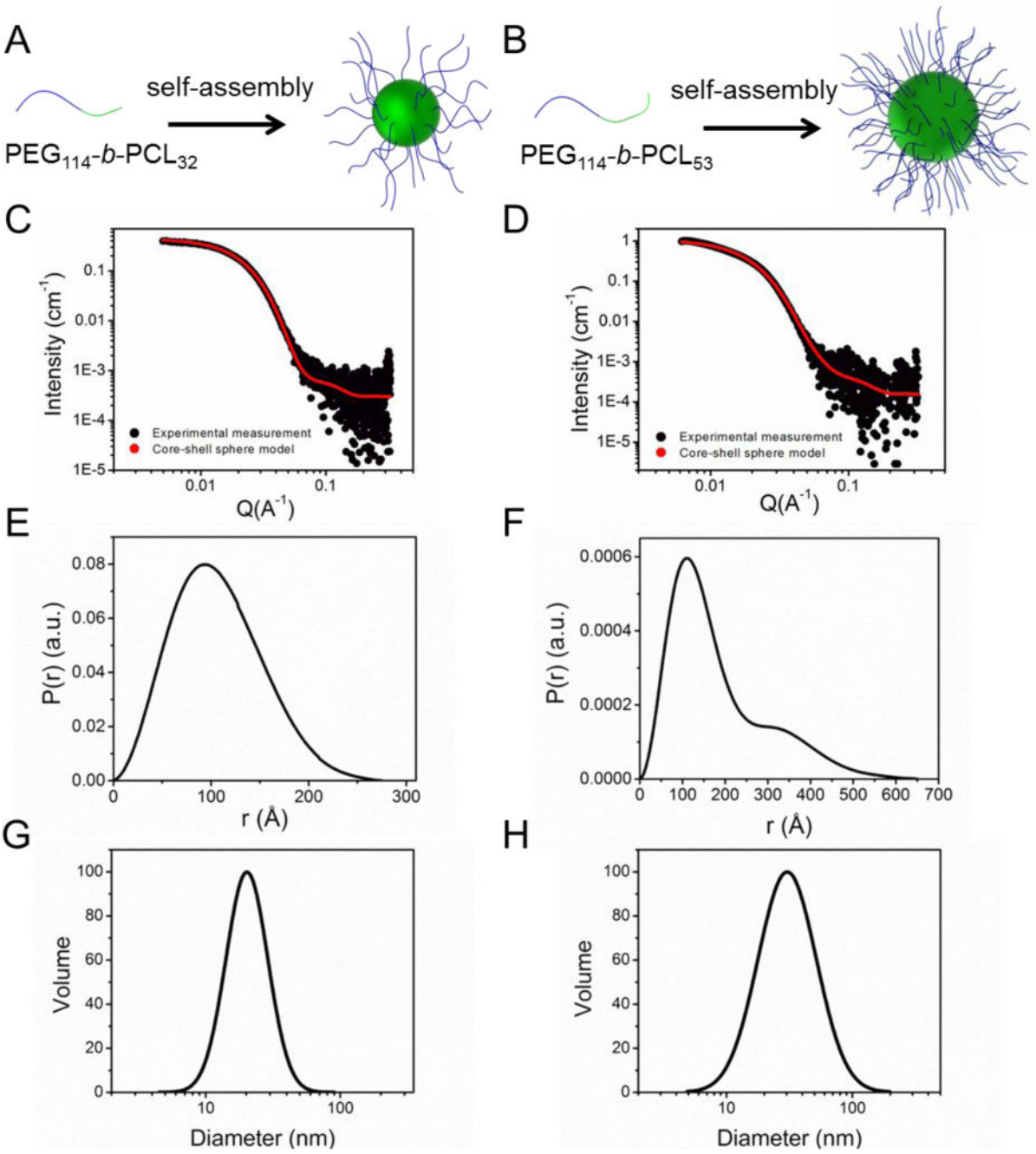

Figure 2.

Structural characterization of micelles formed from linear PEG-*b*-PCL. The PEG length was kept the same and two molecular weights of PCL were used in the study. Data analysis of PEG_{114}-*b*-PCL_{32} micelles (A) and PEG_{114}-*b*-PCL_{53} micelle (B) are columned on the left and right. One-dimensional SAXS data and model fitting (C) and (D), the corresponding *p(r)* distribution function (E) and (F), and the hydrodynamic diameter distribution (G) and (H) for PEG_{114}-*b*-PCL_{32} micelles and PEG_{114}-*b*-PCL_{53} micelles are presented, respectively.

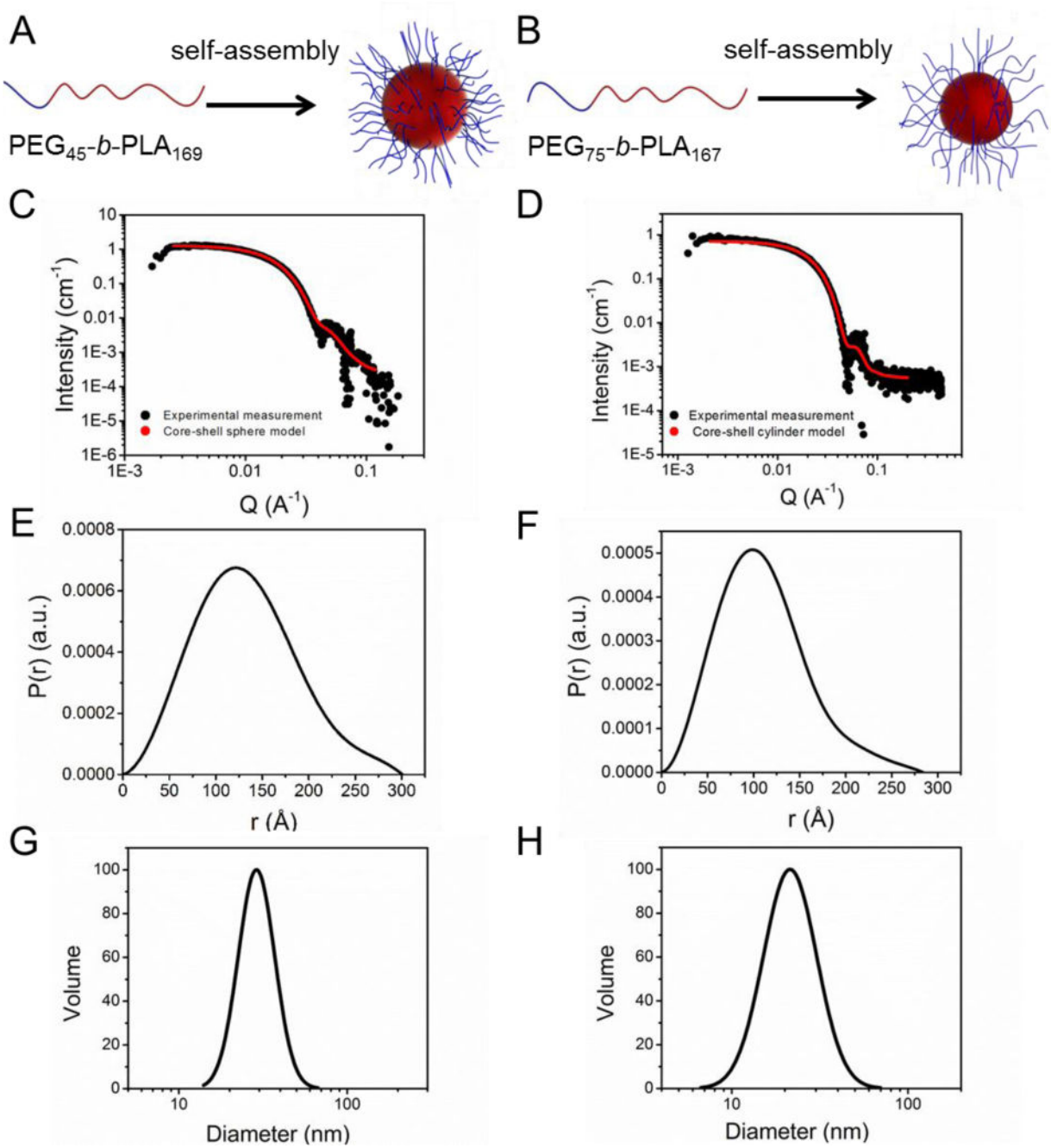

Figure 3.

Structural characterization of micelles formed from linear PEG-*b*-PLA. The PLA length was kept the same and two molecular weights of PEG were used in the study. Data analysis for PEG_{45}-*b*-PLA_{169} micelles (A) and PEG_{75}-*b*-PLA_{167} micelles (B) are columned on the left and right. One-dimensional SAXS data and model fitting (C) and (D), the corresponding *p(r)* distribution function (E) and (F), and the hydrodynamic diameter distribution (G) and (H) for PEG_{45}-*b*-PLA_{169} micelles and PEG_{75}-*b*-PLA_{167} micelles are presented, respectively.

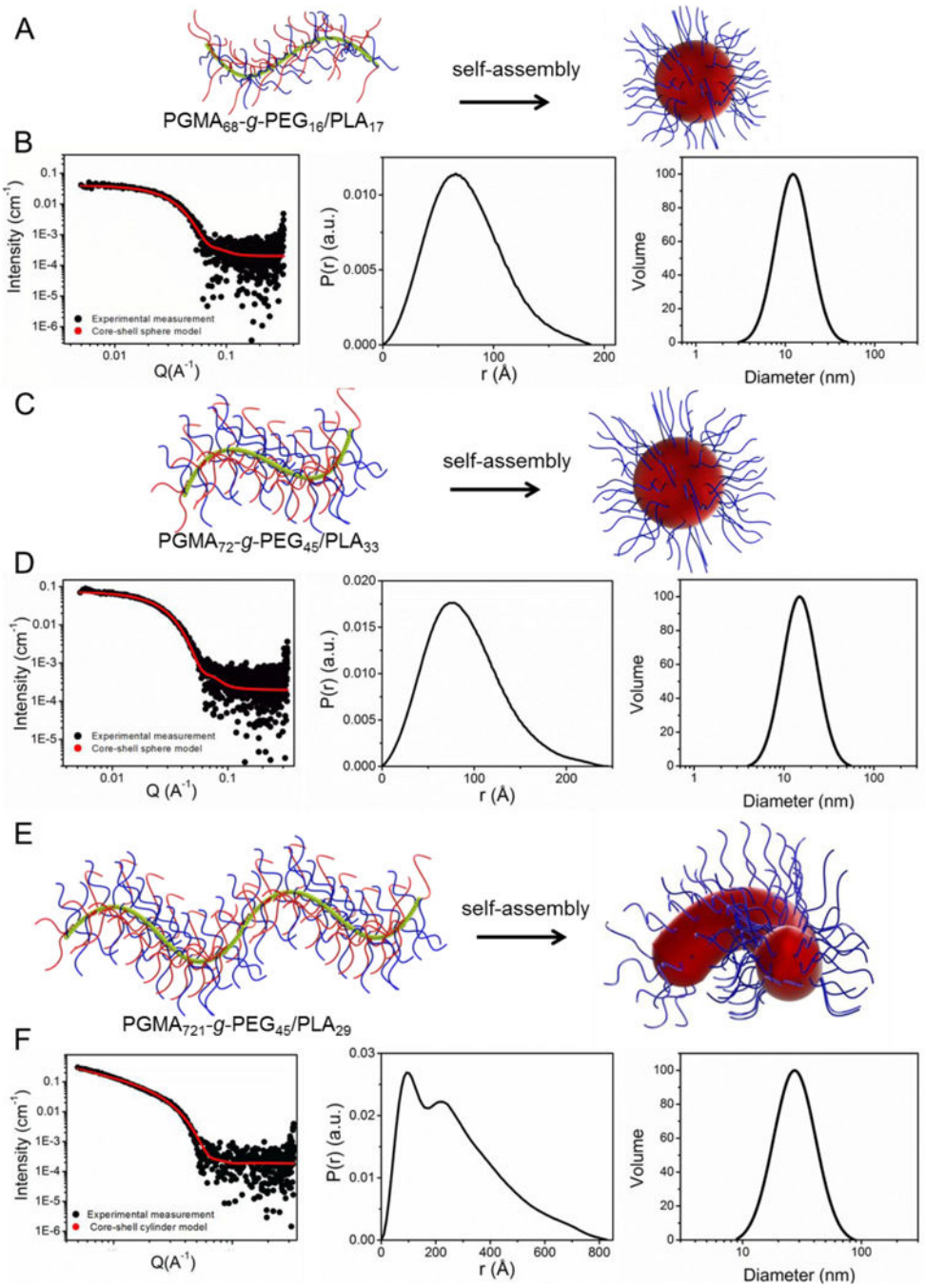

Figure 4.

(A) $PGMA_{68}$-*g*-PEG_{16}/PLA_{17} micelles. (B) Structural characterization of $PGMA_{68}$-*g*-PEG_{16}/PLA_{17} micelles. (C) $PGMA_{72}$-*g*-PEG_{45}/PLA_{33} micelles. (D) Structural characterization of $PGMA_{72}$-*g*-PEG_{45}/PLA_{33} micelles. (E) $PGMA_{721}$-*g*-PEG_{45}/PLA_{29} micelles. (F) Structural characterization of $PGMA_{721}$-*g*-PEG_{45}/PLA_{29} micelles. The left columns of (B), (D), (F) are one-dimensional SAXS data and model fittings. The middle

columns of (B), (D), (F) are the corresponding distance-distribution functions *p(r)*. The right columns of (B), (D), (F) are the hydrodynamic diameter distributions.

Table 1

Molecular-length and concentration information of linear PEG-*b*-PCL and PEG-*b*-PLA polymers and their corresponding micelle R_h and R_g measured by DLS and SAXS respectively.

Polymer	Starting polymer concentration (wt %)	Micelle hydrodynamic radius (R_h; nm)	Micelle radius of gyration (R_g; nm)	R_g/R_h
PEG_{114}-*b*-PCL_{32}	5	10.1	8.0	0.79
PEG_{114}-*b*-PCL_{53}	5	15.0	12.2	0.81
PEG_{45}-*b*-PLA_{169}	1	14.5	10.9	0.75
PEG_{75}-*b*-PLA_{167}	1	10.6	8.1	0.76

Table 2

Structural information calculated from fitting the SAXS data into the core-shell sphere model.

Polymer	R_{core} (Å)	Th_{shell} (Å)	χ^2	Agg#	% PEG_{shell}	No. of PEG chains per nm^2	calcd shell SLD ρ_{shell} ($Å^{-2}$)	Fitted shell SLD ρ_{shell} ($Å^{-2}$)	Diff (%)
PEG_{114}-*b*-PCL_{32}	53.1	46.6	1.50	118	24.88	0.33	9.73E-06	9.63E-06	1.00
PEG_{114}-*b*-PCL_{53}	67.6	42.2	6.64	147	25.70	0.26	9.73E-06	9.62E-06	1.19
PEG_{45}-*b*-PLA_{169}	98.3	33.4	1.42	253	13.23	0.21	9.61E-06	9.67E-06	0.66
PEG_{75}-*b*-PLA_{167}	81.1	24.1	0.39	144	26.50	0.17	9.74E-06	9.88E-06	1.40

Table 3

Molecular-weight and concentration information of brush polymer PGMA-*g*-PEG/PLA and the corresponding micelle R_h and R_g measured by DLS and SAXS, respectively.

Polymer	Starting polymer concentration (wt %)	Micelle hydrodynamic radius (DLS; nm)	Micelle radius of gyration (SAXS; nm)	R_g/R_h
$PGMA_{68}$-*g*-PEG_{16}/PLA_{17}	0.2	6.9	5.7	0.83
$PGMA_{72}$-*g*-PEG_{45}/PLA_{33}	0.27	8.7	6.9	0.79
$PGMA_{72}$-*g*-PEG_{45}/PLA_{33}	2	8.7	7.0	0.80
$PGMA_{721}$-*g*-PEG_{45}/PLA_{29}	0.27	14.9	17.8	1.19
$PGMA_{721}$-*g*-PEG_{45}/PLA_{29}	2	15.8	18.3	1.16

Table 4

Parameter values obtained from fitting the SAXS data of PGMA-*g*-PEG/PLA micelles using core-shell spherical or cylindrical models.

Polymer	R_{core} (Å)	Th_{shell} (Å)	Length (Å)	χ^2	Agg#	% PEG_{shell}	No. of PEG chains per nm^2	calcd shell SLD ρ_{shell} ($Å^{-2}$)	Fitted shell SLD ρ_{shell} ($Å^{-2}$)	Diff (%)
$PGMA_{68}$-*g*-PEG_{16}/PLA_{17}	56.08	9.12	–	1.23	4.06	29.31	0.70	9.77E-06	9.92E-06	1.52
$PGMA_{72}$-*g*-PEG_{45}/PLA_{33}_low	63.94	25.19	–	1.04	3.45	27.62	0.48	9.75E-06	9.52E-06	2.40
$PGMA_{72}$-*g*-PEG_{45}/PLA_{33}_high	64.00	29.09	–	1.11	3.46	22.73	0.48	9.70E-06	9.68E-06	0.19
$PGMA_{721}$-*g*-PEG_{45}/PLA_{29}_low	41.43	27.93	849.99	2.21	1.25	36.14	0.39	9.84E-06	1.03E-05	4.26
$PGMA_{721}$-*g*-PEG_{45}/PLA_{29}_high	42.53	28.14	1004.1	30.29	1.55	37.49	0.40	9.84E-06	1.03E-05	4.99